JOURNAL OF CATALYSIS 23, 131–140 (1971)

Phase Equilibrium in Binary Alloy Crystallites

DAVID F. OLLIS

Department of Chemical Engineering, Princeton University, Princeton, New Jersey 08540

Received February 25, 1971

The role of internal phase boundaries on the stability of two-phase binary crystallites is examined theoretically. It is found that for particles of size 200 Å or less, the critical temperature can be lowered drastically. In particular, an equilibrated alloy particle could be made to remain a single phase at temperatures of interest in catalysis despite the prediction of immiscibility from the bulk-phase diagram. A comparison of experimental results using codeposited alloy films with this prediction from the simple theoretical model is favorable.

The use of binary alloys for investigations into the so-called electronic factor in catalysis by metals has been relatively common (*1*). A general problem in the interpretation of these studies has been the difficulty in obtaining an unambiguous characterization of the alloy catalyst surface composition. Often, this ambiguity has been due to the (possible) simultaneous existence of two phases, i.e., the presence of a miscibility gap in the phase diagram of these binary alloys at the temperatures and compositions of interest.

For example, some recent investigations by Sachtler *et al.* (*2–5*) and Cadenhead *et al.* (*6*, *7*) have exploited the use of chemisorption and physical adsorption studies on copper–nickel alloys. X-Ray diffraction has shown that the evaporated alloy films of Sachtler *et al.* (*2–5*) were generally comprised of two different phases after equilibration at 200°C, indicating a miscibility gap from about 95 to 20% nickel. Similarly, Cadenhead *et al.* (*6*, *7*) observed that the surface composition of granular alloys appeared to differ widely from the average bulk compositions over the greater part of the composition range. While these two studies and others have provided some provocative thoughts about the nature of copper–nickel surfaces in particular, the results derived from studying an equilibrated binary system which is immiscible at nearly all compositions (at moderate temperatures) cannot contribute as greatly as initially hoped to the elucidation of the electronic factor.

The present paper examines the potential role of surface and interfacial free energies of binary alloy crystallites to determine the degree of influence which this surface property may have on the equilibrium phase diagram of the crystallite. In so doing, the crystallite is viewed as a *closed* system to mass transfer of either alloy component.

The creation of a two-phase crystallite from a one-phase (presumably unstable) crystallite is accomplished by decreasing the total free energy per mole of the sample and, neglecting any volume changes, increasing the total surface since a new interface between the resulting phases is created (Fig. 2a, b). For such a transition, the ratio of the surface (destabilizing) to volume (stabilizing) free-energy changes should vary with the inverse of the particle radius. For particles with average composition lying within the miscibility gap of the bulk alloy, there will be a particle radius such that any smaller one-phase particles will experience an increase in total free energy per unit volume upon becoming two-phase and will, therefore, prefer to remain as single-phase systems.

If at a particular temperature useful in catalytic studies (0–400°C), the range of such particle sizes lies in a physically reasonable interval from the point of view of alloy sample preparation, say $\lesssim 100$ Å, it would appear possible to prepare a completely homogeneous series of alloy crystallites over the entire composition range of that binary system, despite the fact that the bulk phase diagram under such conditions exhibits a wide miscibility gap. Contrary to the conclusion of Bond (*1*) that "the ideal (alloy) system for our purposes does not exist," the potential is that any binary system could be made "ideal."

Model System

For the sake of a simple calculational system which contains the central features of interest, we consider the alloy crystallite shown in Fig. 2a and b. Subscripts 0, 1, and 2 refer to the initial homogeneous crystallite, and the two final phases into which the original phase may separate. The phase diagram of binary solid systems are often shown in terms of convenient temperature vs composition ($T - x$) diagrams (e.g., Fig. 1). The model chosen is that of a regular solution for all three possible phases: The heat of mixing is determined by a single interaction parameter, Ω, but the entropy of mixing has the same form as for an ideal solution (*9*). For any given phase, then, the enthalpy of mixing per mole and entropy of mixing per mole are given by Eqs. (1) and (2):

$$h_i = \Omega x_i(1 - x_i), \tag{1}$$

$$S_i = -R(x_i \ln x_i + (1 - x_i) \ln (1 - x_i)). \tag{2}$$

We also neglect any volume changes due to mixing, and assume that the molar volumes of component A and B are equal. $v_A = v_B = v$.

If the crystallite in Fig. 2a separates into the two-phase system in Fig. 2b, the resulting free-energy change is composed of two parts: a volume term and a surface term. Taking y as the fraction of the original volume (or moles) becoming phase 1, the volume contribution to the free-energy change per unit volume is

$$\Delta g_v = yg_1 + (1 - y)g_2 - g_0, \tag{3}$$

where g_1, g_2, and g_0 are the volume free energies of mixing of the three phases (referred to the pure components). The surface contribution to the free-energy change is the contribution due to the phase interface in Fig. 2b (assuming that the surface tension is not a function of composition). This term is simply the surface tension of the 1–2 interface times its area divided by the total number of moles in the crystallite:

$$\Delta g_s = \sigma \cdot A/N, \tag{4}$$

where σ = surface tension; A = interfacial area; and N = total moles in crystallite. The total moles, N, is simply $\frac{4}{3}\pi r^3/v$, where v is the molar volume, and r is the crystallite radius. The interface is assumed

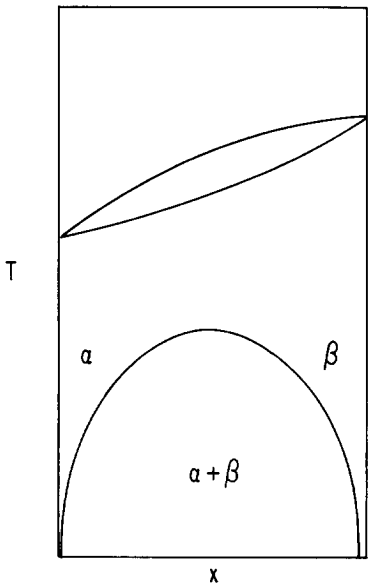

Fig. 1. Phase diagram of a binary system with a miscibility gap in the solid region.

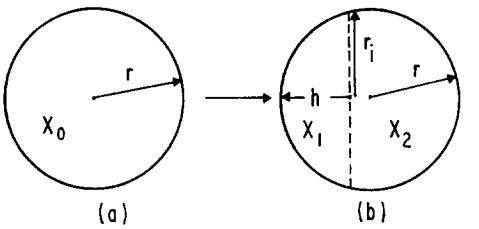

Fig. 2. Schematic diagram of phase transition from phase 0 to phases 1 and 2 for a spherical crystallite.

to be planar (this approximation is discussed later), and is thus a circle of radius r'.

Since the free energy of mixing for any given phase is $g_{mix} = h_{mix} - Ts_{mix}$, Eqs. (1) and (2) combined with Eqs. (3) and (4) yield the total free-energy change per mole, Eq. (5):

$$\begin{aligned}\Delta g &= \Delta g_v + \Delta g_s \\ &= yg_1 + (1-y)g_2 - g_0 + A\sigma/N \\ &= [yh_1 + (1-y)h_2 - h_0] - T[yS_1 + (1-y)S_2 - S_0 + A\sigma/N \\ &= \Omega[yx_1(1-x_1) + (1-y)x_2(1-x_2) - x_0(1-x_0)] \\ &\quad - T[y(x_1 \ln x_1 + (1-x_1)\ln(1-x_1)) + (1-y)(x_2 \ln x_2 \\ &\quad + (1-x_2)\ln(1-x_2)) - x_0 \ln x_0 - (1-x_0)\ln(1-x_0)] \\ &\quad + \frac{3}{4}\sigma v (r')^2/r^3 \end{aligned} \tag{5}$$

A component balance for component A, represented by x_i for each phase, yields an expression for y in terms of the initial and final compositions for the three phases.

$$y = \frac{x_0 - x_2}{x_1 - x_2}. \tag{6}$$

Next, the radius of the phase interface is also expressed in terms of the three compositions x_0, x_1, and x_2. The volume of the lesser segment in Fig. 2b is given by

$$(\text{vol})_1 = \frac{\pi}{3} h^3(3r - h), \tag{7}$$

where h is height of the spherical segment ($h < r$), and the volume fraction is thus

$$y = \frac{1}{4}\left(\frac{h}{r}\right)^2\left(3 - \frac{h}{r}\right) = \frac{z^2}{4}(3 - z), \tag{8}$$

where $z = h/r$; and $0 < z < 1$.

Equating (8) and (6) yields a cubic equation for z, the dimensionless height:

$$z^2(3 - z) - 4\left(\frac{x_0 - x_2}{x_1 - x_2}\right) = 0. \tag{9}$$

The root of Eq. (9) lying between 0 and 1 is given by

$$z = \cos\left(\frac{\theta}{3} - \frac{2\pi}{3}\right), \tag{10}$$

where $\theta = \arccos(1 - 2y)$; and $y \lesssim \frac{1}{2}$. (The problem is symmetric about $y = \frac{1}{2}$.)

Since $(r')^2 = r^2 - (r-h)^2 = h(2r - h)$, the term r'/r is given by

$$\left(\frac{r'}{r}\right)^2 = \left(\frac{h}{r}\right)\left(2 - \frac{h}{r}\right) = z(2 - z),$$

and the surface contribution to the free-energy change is the expression in Eq. (11).

$$\Delta g_s = \frac{3}{4}\frac{\sigma N_0}{r}\left(\frac{r'}{r}\right)^2 = \frac{3}{4}\frac{\sigma N_0 z(2-z)}{r}. \tag{11}$$

Substituting Eqs. (6) and (11) into Eq. (5) results in the working equation for the free-energy change of the regular solution crystallite on going from Fig. 2a to Fig. 2b.

$$\begin{aligned}\Delta g = \Omega &\left[\left(\frac{x_0 - x_2}{x_1 - x_2}\right)x_1(1-x_1) + \left(\frac{x_1 - x_0}{x_1 - x_2}\right)x_2(1-x_2) - x_0(1-x_0)\right] \\ &- T\left[\left(\frac{x_0 - x_2}{x_1 - x_2}\right)(x_1 \ln x_1 + (1-x_1)\ln(1-x_1)) \right. \\ &+ \left(\frac{x_1 - x_0}{x_1 - x_2}\right)(x_2 \ln x_2 + (1-x_2)\ln(1-x_2)) \\ &\left. - x_0 \ln x_0 - (1-x_0)\ln(1-x_0)\right] \\ &+ \frac{3}{4}\frac{\sigma N_0}{r} z(2-z), \end{aligned} \tag{12}$$

where $z = z(x_0, x_1, x_2)$.

When Δg is less than zero, the phase transition shown in Fig. 2 is favored, and the two-phase crystallite is the phase of lowest free energy. If Δg is positive, the single-phase crystallite is most stable. Since the interfacial boundary contributes a positive term to the free-energy change per unit volume which is inversely proportional to the particle radius, for any value of T, x_0, x_1, and x_2 (and Ω and v), there is some value of r for which all alloy particles of radius r or less will prefer to be a single phase which, in the case of this simple model, will be homogeneous.

The curve in the phase diagram of Fig. 1 which separates the region of two solid phases from the single-phase region is the curve defined by Eq. (12) when the free-energy change is zero. This curve is only a function of initial (or average) composition and thermodynamic property Ω for bulk samples of regular solutions (radius equal to infinity).

$$T_{r=\infty} = T(\Omega, x_0). \tag{13}$$

For a finite particle with a nonzero surface tension, the curve becomes a function of the surface tension, the radius, and the molar volume in addition to the original variables of Ω and initial composition.

$$T_{r\neq\infty} = T(\Omega, x_0, \sigma, r, v). \tag{14}$$

For the remaining discussion and presentation of results, the curve in Eq. (14) was calculated by a trial and error interation procedure in the following two-step algorithm: Choose $\Omega = 2R \cdot 1500$ ($\cong 6$ kcal/mole), $v = 10$ Å^3. Given values for the variables x_0, Ω, σ, v, and an initial temperature (assumed).

(a) Search over all allowable values of x_1 and x_2 to find the pair of values (x_{1m}, x_{2m}) which maximize the free-energy change in Eq. (12).

(b) Set the left hand side of Eq. (12) equal to zero and solve for a new temperature using the values of x_{1m} and x_{2m} from part (a). Return to (a) to search for revised values of x_{1m} and x_{2m} above.

The iteration is repeated until satisfactory convergence is obtained. The final values of x_{1m} and x_{2m} are the compositions of the two phases into which a phase of composition x_0 will separate at the final temperature calculated in part (b) of the iterations.

Since the location of the interface is unknown initially, the values of x_1 and x_2 must be independently varied; Eq. (6) guarantees that for any values of x_1 and x_2 such that $0 \leq x_1 < x_0 < x_2 \leq 1$, the conservation requirement is satisfied. At equilibrium, x_1 and x_2 are not independent.

It is illustrative to vary either surface tension or radius while holding the other constant.

In order to determine what values of surface tension (or its numerical equivalent, surface free energy) are most relevant, consider the literature data in Table 1. By far the smallest internal boundary free energy, ΔG^b, is that found for a coherent twin boundary interface. This interface forms when the crystal structures of each phase are identical and the dividing boundary is a twinning (or mirror) plane. When the two-phase structures are oriented as twins but the boundary is not the twinning plane, a noncoherent twin interface results with higher interfacial free energies (440

TABLE 1
INTERFACIAL ENERGIES FOR METAL CRYSTALS (*29*)

Crystal	Interface	Interfacial free energy (ergs/cm^2)
Copper	Coherent twin	25[a]
Copper	Noncoherent twin	440[b]
Copper	High angle	600[c]
Iron	Coherent twin	187[d]
Iron	Noncoherent twin	705[d]
Iron (γ)	High angle	850[e]
Iron (α, 4% Si)	High angle	760[e]

[a] R. L. Fullman, *J. Appl. Phys.* **22,** 448 (1951).
[b] R. L. Fullman, *J. Appl. Phys.* **22,** 456 (1951).
[c] N. A. Gjostein, and F. N. Rhines, *Acta Met.* **7,** 319 (1959).
[d] C. G. Dunn, F. W. Daniels, and M. J. Bolton, *J. Metals* **2,** 368 (1950).
[e] L. H. Van Vlack, *J. Metals* **3,** 25 (1951).

ergs/cm² and 705 ergs/cm² for Cu and Fe, respectively).

In the more general case, no twinning orientation is present, the two grains of identical structure and composition are randomly oriented with respect to one another. The usually consequent high-angle grain boundary has still higher energies (600 ergs/cm² for Cu and 850 ergs/cm² for Fe).

The interface between two binary phases which differ both in composition and structure has a surface energy term which is difficult to calculate a priori for a number of reasons. Swalin (*9*) points out, however, that the measured interfacial free energies for such systems are about the same as those for a high-angle grain boundary between two grains of one of the phases, i.e., a boundary between two randomly oriented phases of identical structure and composition. Some relevant data summarized by Swalin are shown in Table 2.

For calculational purposes, it is of interest to consider a range of interfacial free energies which may be characteristic of the different possible transition metal alloys. Two general features are useful in this regard:

(a) In the simplest theory, the solid–vacuum interfacial free energy, ΔG^{sv}, is proportional to the latent heat of sublimation, H_s.

(b) The internal boundary free energy for high-angle grain boundaries (and thus also for boundaries separating two different crystal phases, Table 2) is roughly one-third of the solid–gas interfacial energy: $\Delta G^b/\Delta G^{sv} \sim \frac{1}{3}$.

(For most boundaries, the derivative $\delta(\Delta G^b)/\delta\theta$ is small if the angle of twist or tilt, etc., between the two adjoining structures is fairly large (high-angle case). For such cases, internal boundary free energies are not strongly dependent on the exact relative phase orientations.)

The refractory transition metals have heats of sublimation on the order of twice those of the iron and copper: e.g., in kcal per mole, Nb(185), Mo(155), Ta(185), W(202), Re(189) vs Fe(99) and Cu(81). The two previous guidelines suggest that about 1200 ergs/cm² is a reasonable grain-boundary value for ΔG^b between two different phases of a refractory metal alloy.

The values for the interfacial free energy of the phase boundary in Fig. 2b were taken as 0, 300, 600, and 1200 ergs/cm² to be used in Eq. (12). These values may be crudely associated with an infinite particle (radius going to infinity), a twin noncoherent boundary, and a high-angle grain boundary for Group VIII and refractory metals, respectively.

The solution of Eq. (14) under various assumed values for internal boundary free energy and particle radius results in important shifts of the T vs x_0 curve defined by Eq. (14) for which the total free-energy

TABLE 2

RELATIVE INTERFACE FREE ENERGIES (*25*)

System	Interface between		Grain boundary used as a comparison interface, D	$\frac{\Delta G_{AB}{}^b}{\Delta G_D{}^b}$	T(°C)
	Phase A	Phase B			
Cu–Zn[a]	α-fcc	β-bcc	α/α	0.78	700
			β/β	1.00	700
Cu–Al[a]	α-fcc	β-bcc	α/α	0.71	600
	α-fcc	γ-complex cubic	γ/γ	0.78	600
Fe–C[b]	α-bcc	Fe_3C	α/α	0.93	690
	α-bcc	γ-fcc	α/α	0.71	750

[a] C. S. Smith, *Trans. AIME* **175**, 15 (1948).

[b] Ref. (*25*).

change is zero. Within relatively minor variations of 1–2 at. %, the *final* compositions 1 and 2 into which the phase 0 could separate were found to be independent of these two variables of surface tension and radius. In the following diagrams, the T vs x_0 curves for finite surface tension and finite radius are the highest temperatures at which the crystallite of radius r and surface tension σ will begin to be unstable with respect to formation of a two-phase particle. When decomposition is predicted, the composition of the resulting phases 1 and 2 is essentially that expected for the same temperature using the T vs x_0 curve for the bulk alloy (infinite radius or vanishing surface tension, curve 1 in Figs. 3, 4, and 5).

The effect of interfacial free energy on the solution of Eq. (14) (or, equivalently, Eq. (12) when Δg equals zero) is shown in Figs. 3 and 4 for radii of 1000 and 50 Å. There is a noticeable effect on the $T - x_0$ curves even for the large (2000 Å) crystallite, and a drastic effect for the smaller (100 Å) particle case even with a relatively low internal boundary free energy of 300 ergs/cm². If the maximum interfacial energy value of 1200 ergs/cm² is assumed, the minimum temperature to which an equimolar 100-Å crystallite can cool without phase separation is nearly halved, being cut from 1500°K (arbitrarily assumed critical temperature for the bulk alloy) to 790°K.

Fixing the interfacial energy and varying the particle diameter results in the $T - x_0$ curves shown in Fig. 5. Again the influence of particle size becomes pronounced for particles with radii of 100 Å or less.

The curves in Figs. 3, 4, and 5 are easily scaled to other temperatures. For a regular solution in an infinite particle (topmost curves, in Figs. 3, 4, and 5), the maximum temperature associated with the miscibility gap occurs at $x = 0.5$. This critical temperature, T_c, is equal to $\Omega/2R$, where Ω is the interaction parameter in Eq. (1), and R is the gas constant. Thus $\Omega = 2RT_c$, and the three parameters T_c, T, and surface tension σ can all be scaled together (as is seen in Eq. (12)). For example, if $T_c =$

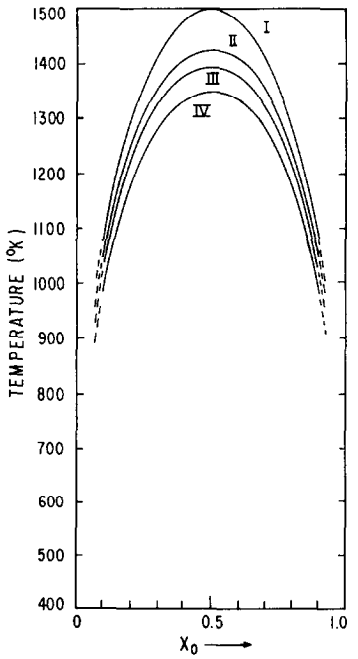

FIG. 3. Effect of internal boundary free energy on the phase diagram of a regular binary solution ($T_c = 1500$°K), crystallite diameter = 2000 Å. ΔG^b(ergs/cm²) = 0(I), 300(II), 600(III), 1200(IV).

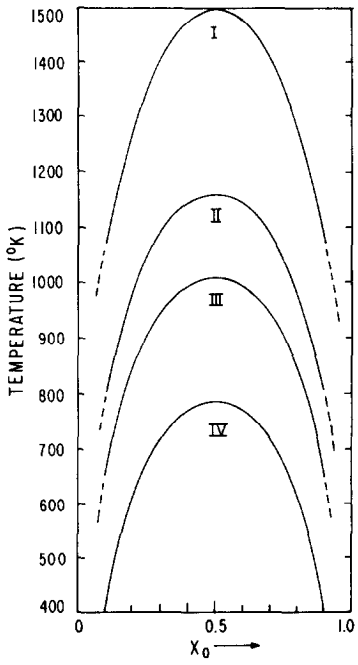

FIG. 4. Effect of internal boundary free energy on the phase diagram of a regular binary solution ($T_c = 1500$°K), crystallite diameter = 2000 Å. ΔG^b(ergs/cm²) = 0(I), 300(II), 600(III), 1200(IV).

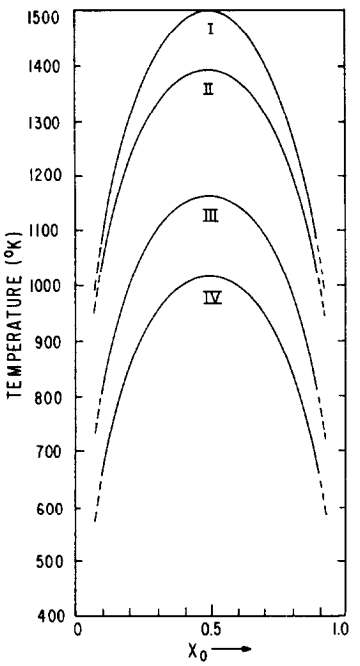

FIG. 5. Effect of crystallite diameter on phase diagram of regular solution ($T_c = 1500°K$, $\Delta G^b = 600$ ergs/cm^2). d(Å) $= \infty$(I), 2000 Å(II), 200 Å(III), 100 Å(IV).

750°K (as is roughly true for Cu–Ni alloys) and the surface tension is about 600 ergs/cm^2 (a high-angle grain boundary for Cu), curves I and IV in Fig. 4 indicate that the change in temperature at which an equimolar 100-Å-diameter crystallite should undergo a phase transition is $\frac{1}{2}(710°K) = 355°K$. The resulting "critical temperature" for the crystallite is $750 - 355 = 395°K$ or 122°C. Where an equilibrated bulk sample of this alloy at 425°K would exhibit phase immiscibility over more than 90% of the composition range, a 100-Å-diameter particle with the assumed internal boundary free energy of 600 ergs/cm^2 would remain a single phase regardless of its average composition.

If now an evaporated film of such crystallites is prepared and studied at 150°C in such a manner as to avoid major sintering, a completely homogeneous series of alloy catalysts could be obtained for this system, despite the fact that the components are nearly totally immiscible in bulk samples at this temperature.

Simplifying Assumptions

The relation of the results summarized in Figs. 3, 4, and 5 to real systems may be discussed by considering three items: the shape of the interface, the thickness of the interface, and the applicability of the regular solution model.

Interfacial boundary geometry: The assumption of a flat boundary between the two phases in Fig. 2b is strictly a calculational convenience. If phase 1 or 2 is a small fraction of the original phase 0 present initially (y near 0 or 1 in Eq. (6)), a curved boundary something of the order of ellipsoidal or spherical would perhaps be more likely. (The governing considerations which would determine the shape when y is near one or zero are exactly analogous to those governing the shape of coherent and incoherent embryos in nucleation in solids: the elastic properties of each phase, the variation in surface tension with composition and orientation, and the lattice disregistry between the two phases (10).) However, near $y = 0.5$, a flat boundary is the expected minimum energy form, assuming that the gas–solid surface tensions in Figs. 2a and 2b are identical. Since our primary concern is in obtaining one-phase crystallites for all compositions, it is the determination of the solution of Eq. (14) near $y = 0.5$ which is crucial. In this respect, a flat interface is justifiably assumed.

A balancing of surface tensions and internal boundary tension would yield a small groove around the external particle surface, thus slightly increasing the external surface area and decreasing the internal surface area. Even for $\sigma^b \sim \frac{1}{3}\sigma^{sv}$, the angle α measuring the deviation from a straight line of the joining 1 and 2 surfaces is only about 9°:

$$\sigma^b = 2(\sin \alpha)\, \sigma^{sv}$$

$$\sin \alpha = \frac{1}{6}$$

$$\therefore \alpha \simeq 9.2°$$

The angle change is a small one and probably results in only a small change in the $T - x_0$ curves since surface of ΔG^{sv} values three times or more that of ΔG^b must be

created at the groove in order to reduce the internal boundary area, A.

Thickness of interface. The interface between the (assumed) homogeneous phases is necessarily of some finite thickness in contrast to the interface of negligible volume assumed in Eq. (12). Cahn and Hilliard (*11–13*) have treated such finite interface systems extensively by drawing on analogous phenomena in interfaces separating domains of magnetic (*14*) or ferroelectric (*15*) materials. Since the use of experimental surface free energies in the present paper will automatically include both "surface" and "volume" contributions associated with a finite interface, this interfacial volume should have been subtracted from the initial volume prior to calculation of the volume free-energy contributions from phases 1 and 2. As such a correction would decrease the total, negative, free-energy change favoring formation of a two-phase system, the results in Figs. 3–5 are conservative in this regard. Inclusion of a finite interface in the preceding calculations would simply amplify the predicted differences for the different cases.

Regular solution assumption: Equations (1) and (2) represent a simple model of a binary system exhibiting the one feature of interest, a miscibility gap in the solid region. The author does not feel that inclusion of strain considerations and various more realistic excess enthalpy and entropy of mixing terms would seriously change the qualitative predictions of the previous discussion.

Application to Catalysis

The predictions evolved from the regular solution model may bear on our understanding of catalysis at surfaces only insofar as the following two points may be answered affirmatively:

(1) Are there real systems known to exhibit the effects predicted above?

(2) Is the surface composition related in a known manner to the (local) bulk composition?

These questions are now considered in light of some thin-film and field-ion-microscope studies of this last decade.

1. *Real Systems*

Kneller (*16*) was able to produce metastable solid solutions of Fe–Cu and Co–Cu by simultaneous vapor deposition of both metals on a cool substrate. These alloys exhibited single-phase behavior at room temperature; subsequent heating yielded decomposition into two phases. A number of single-phased-metastable binary systems have been produced by Mader (*17*) via deposition onto an 80°K substrate, followed by heating. He found that, when the ratio of the larger to smaller metal diameter exceeded $\sim$1.1, an amorphous structure was often formed. Heating the amorphous structure yielded changes at two temperatures, T_1 and T_2. At T_1, crystallization into a single homogeneous phase was observed. At $T_2(>T_1)$, the single-phase system decomposed into two phases as expected from the equilibrium diagram for the bulk system. A summary of some binary metal pairs possessing bulk-phase diagrams indicating a miscibility gap and also yielding such metastable single-phase alloys at modest temperatures is given in Table 3 (*17*).

A central observation by Mader (*19*) arose from a beautiful study of Co + 38 at. % Au codeposited at 80°K. In the temperature "range where the crystalline metastable phase exists . . .", "The most conspicuous change in this metastable phase is grain growth. Microscopic observations indicate that the average grain size increases from about 20 to several hundred angstroms in the temperature range between the two annealing stages" (*19*). Thus the single-phase first appears at temperature $\sim T_1$ with crystallites of the order of 20 Å in diameter. These crystallites grow and coalesce into larger crystallites until, at a size of "several hundred angstroms" and a temperature of T_2, decomposition into two phases occurs.

The single-phased systems observed by Mader *et al.* (*17, 19*) and also by Chopra (*20*) have been termed metastable by these investigators and have been explained as due to a short-range ordering prior to the

TABLE 3

APPROXIMATE COMPOSITION RANGES AND FIRST AND SECOND CRYSTALLIZATION TEMPERATURES (T_1 AND T_2, RESPECTIVELY) FOR SINGLE-PHASE METASTABLE AND AMORPHOUS ALLOYS OF SOME SYSTEMS CODEPOSITED AT 80°K[a]

System A-B	Atom-size ratio r_B/r_A	Percentage of composition range yielding metastable (fcc) single-phase films at deposition temperature	Percentage of composition range yielding amorphous films at deposition temperature	T_1, °K	T_1/T_m[b]	T_2/T_m[b]
Co–Cu	1.02	100	No			0.45
Co–Au	1.11	<25 (both)	>25 (both)	~430		0.36
Cu–Au	1.12	100 (disordered)	No			
Cu–Ag	1.13	<37 (both)	>37 (both)	~370	0.28	0.38
Co–Ag	1.15	No	100	~180	0.12	0.24
Cu–Sn	1.18		>30	~150	0.1	
Cu–Mg	1.25	<18 Cu(fcc) <10 Mg(hcp)	>18 Cu >10 Mg	~400	0.35	
Fe–Au[c]	1.11		20–60 Au	~200	0.13	
Gd–Au[c]	1.13		50–80 Gd	~480	0.3	

[a] Summarized by Chopra, "Thin-Film Phenomena" (*20*).

[b] T_m refers to the average of the melting points of the components.

[c] S. Mader, unpublished results.

activated decomposition step occurring at the higher temperature T_2. In light of the regular solution model discussed in the text of the present paper, it seems reasonable to expect that (1) the 20-Å particles are single phase *because that is the equilibrium configuration* for such small crystallites at temperature T_1 as is suggested from Figs. 4 and 5, and (2) in the absence of further sintering and grain growth, these small "metastable" particles are not metastable at all: they *are* the equilibrium state of 62% Cu/38% Au in an ~20-Å state of subdivision. The present theory thus appears to satisfactorily explain the behavior of the "metastable" systems in Table 3 or, conversely, these real binary pairs seem indeed to exhibit the predicted effects shown in Figs. 3, 4, and 5.

2. *Surface vs Bulk Composition*

The fundamental problem is to measure the surface composition for an alloy of known bulk composition without resorting to calibration by the very process one wishes eventually to understand: chemisorption on an alloy surface. Field-ion microscopy seems to provide some information, but further progress via such independent techniques will be difficult. Field evaporation of surface atoms from *fully ordered* sample tips of PtCo (Mueller (*21*)), Pt_3Co (Tsong and Mueller (*22*)), and Ni_4Mo (Newman and Hren (*23*)) yields surfaces with composition simply that expected by cutting a sphere from a solid, perfectly ordered sample. Random or uniformly disordered alloy solutions do not appear to develop crystallographically perfect planes; at the present time, it is not known whether this fact is associated with the field-evaporation technique, or, more interestingly, with surfaces of random or disordered alloys in general. As a consequence, FIM techniques have not yielded surface compositions of such samples.

More research in this area relating surface and bulk compositions is clearly in order.

CONCLUSION

The present paper has predicted that a binary regular solution system can potentially be made to remain in one single phase at temperatures well below the critical temperature for bulk samples by produc-

ing the alloy sample as very small crystallites (less than 100-Å radius). Certain experimental observations by Mader in particular seem to strongly support the predictions of the simple regular solution model developed in the present paper (although his alloys are not perfect regular solutions). These observations further suggest an appropriate experimental approach to be used in future alloy work, viz., codeposition on cooled surfaces *in vacuo* as practiced by both Mader (*17*, *19*) and Sachtler (*2–5*, *24*).

The availability of such uniform samples over the full range of composition would clearly offer the potential of finally achieving an understanding of the electronic factor in catalysis by metals.

Acknowledgment

This work was supported by a grant from the National Science Foundation (NSF-GK-5219).

References

1. Bond, G. C., "Catalysis by Metals," pp. 476–484. Academic Press, New York, 1962.
2. Sachtler, W. M. H., and Dorgelo, G. J. H., *J. Catal.* **4**, 654 (1964).
3. Sachtler, W. M. H., Dorgelo, G. J. H., and Jongpier, R., "Proceedings of the International Symposium on Basic Problems in Thin Film Physics," Clausthal, 1965, p. 218. Vandenhoeck and Ruprecht, Göttingen, 1966.
4. Sachtler, W. M. H., and Jongpier, R., *J. Catal.* **4**, 665 (1965).
5. van der Plank, P., and Sachtler, W. M. H., *J. Catal.* **12**, 35 (1968).
6. Cadenhead, D. A., Wagner, N. J., and Thorp, R. L., *Proc. Int. Congr. Catal., 4th 1968* **2**, 453 (1969).
7. Cadenhead, D. A., and Wagner, N. J., *J. Phys. Chem.* **72**, 2775 (1968).
8. Ehrlich, G., and Hudda, F. G., *J. Chem. Phys.* **44**, 1039 (1966).
9. Swalin, R. A., "Thermodynamics of Solids," pp. 156–213. Wiley, New York, 1962.
10. Burke, J., "The Kinetics of Phase Transformations in Metals," pp. 132–151. Pergamon Press, New York, 1965.
11. Cahn, J. W., and Hilliard, J. E., *J. Chem. Phys.* **28**, 258 (1958).
12. Cahn, J. W., and Hilliard, J. E., *J. Chem. Phys.* **31**, 688 (1959).
13. Bloch, F., *Z. Phys.* **74**, 295 (1932).
14. Mitsui, T., and Furnichi, J., *Phys. Rev.* **90**, 193 (1953).
15. Bardeen, *Phys. Rev.* **94**, 554 (1959).
16. Kneller, E., Jr., *J. Appl. Phys.* **33**, 1355 (1962), **35**, 2210 (1964).
17. Mader, S., *J. Vac. Sci. Technol.* **2**, 35 (1965).
18. Nowick, A. S., and Mader, S., *IBM J. Res. Develop.* **9**, 358 (1965).
19. Mader, S., in "The Use of Thin Films for Physical Investigations" (J. C. Anderson, ed.), p. 433. Academic Press, New York, 1966.
20. Chopra, K. L., Ledgemont Laboratory Report. TR-179, August, 1968. See also Chopra, K. L., "Thin Film Phenomena," p. 205. McGraw-Hill, New York, 1969.
21. Mueller, E. W., *in* "Field Emission Symposium, 8th" Williamstown, Mass. (August 1961); *Bull. Amer. Phys. Soc.* **7**, 27 (1962).
22. Tsong, T. T., and Mueller, E. W., *J. Appl. Phys.* **38**, 3531 (1967).
23. Newman, R. W., and Hren, J. J., *Phil. Mag.* **16**, 211 (1967).
24. Swalin, R. A., "Thermodynamics of Solids," pp. 205–206; cited from Tables 12.4 and 12.5. Wiley, New York, 1962.
25. Smith, C. S., "Imperfections in Nearly Perfect Crystals" (W. Shockley, ed.), Wiley, New York, 1952.